RSC Advances

ROYAL SOCIETY OF CHEMISTRY

www.rsc.org/advances

Synthesis of Au- MWCNT-Graphene hybrid composite for rapid detection of H_2O_2 and glucose

Pranati Nayak, Santhosh P N and S Ramaprabhu

Alternative Energy and Nanotechnology Laboratory (AENL), Nano Functional Materials Technology Centre (NFMTC), Department of Physics, Indian Institute of Technology Madras, Chennai – 600036, India

Email:- ramp@iitm.ac.in

Abstract

We report the fabrication of a novel amperometric biosensor based on narrow sized Au nanoparticles (~4nm) decorated multiwalled carbon nanotube-solar exfoliated graphene (MWCNTs-sG) hybrid composite as an enzyme immobilizer and sensing matrix for hydrogen peroxide (H_2O_2) and glucose. Au nanoparticles decorated MWCNTs-sG hybrid composite was synthesized by a green technique using focused solar radiation and characterized. The fabricated biosensor displays good catalytic response towards H_2O_2 redox reaction with wide linearity ranging from 1mM to 62mM and with fast amperometric response with a response time of < 1s. The limit of detection is calculated to be 13µM (S/N= 3). While employed for enzymatic glucose detection, the sensor shows excellent fast response with a response time of ~0.1s towards glucose over a concentration range from 50µM to 20mM with a limit of detection 2.48µM. Using Michaelis-Menton enzyme kinetics, the apparent Michaelis-Menton constant (K_m) is estimated as 1.07mM which depicts high affinity of the enzyme biosensor towards substrate. This is due to the synergistic combination of small sized Au nanoparticles on graphene layers in the presence of MWCNTs as conducting spacer which intern enhances the electrochemically active surface area. This favors better enzyme immobilization on the hybrid material and promotes the direct electron transfer mechanism. In addition, the biosensor shows satisfactory selectivity over coexisting interference species like UA, AA, DA and good reproducibility. On the basis of easy large-scale green synthesis technique of the sensor material, its ultrafast response, wide range linearity and low detection limit, the present biosensor promises potential applications in electrochemical biosensing.

1. Introduction

Since the advent of Clark and Lyons pioneer work on incorporation of enzyme in electrochemical detection of glucose in 1962, enzymatic glucose sensing have been a subject of numerous studies owing to not only for clinical treatment of diabetes mellitus but also for its application in food security, biotechnology and environmental pollution control.[1-2] This trend has been stimulating scientific community in the development of biosensors of fast response, high sensitivity, good selectivity, long term stability and low cost. Electrochemical enzymatic glucose detection basically involves the conversion of glucose to gluconolactone in presence of glucose oxidase (GOD) enzyme releasing H_2O_2. Then applying a working potential to the bio electrode results H_2O_2reduction at electrode-electrolyte interface to give proton (H^+), electrons (e^-) and O_2.[3] This contributes an electric current flow proportional to the concentration of H_2O_2 which intern relates to glucose concentration. Here the catalytic activity of the bioelectrode plays a major role in enhancing the sensor current output, linearity range, selectivity and decreasing its response time.[4 -5] In past few decades, a lot of effort has been given in improving the analytical performance of the biosensor by incorporating conducting nanomaterials as the active site for effective enzyme immobilization and direct electron transfer at enzyme - electrode interface. In this regard, nanostructure materials like carbon nanotubes and graphene have been receiving tremendous attention in electrochemical biosensing due to its intriguing physicochemical properties including high surface to volume ratio, enhanced catalytic activity and excellent fast charge transfer properties.[6-10]

Graphene, composed of two dimensional honeycomb arrangements of sp^2- bonded carbon atoms is a rising star in materials research. The novel properties of graphene includes large specific

surface area, high electrical conductivity, mechanical strength, superior thermal and chemical stability which makes it robust for varieties of technological applications such as nanoelectronics, photovoltaic, nanophotonics, field effect transistors, energy storage/production related materials and chemical/biological sensors.[11-13] Owing to its excellent electrochemical activity and charge transport properties, graphene based hybrids have been reported as an excellent transducer material in electrochemical biosensors.[14] Numerous efforts have been made to tailor the properties and hence improve the performance by incorporating different metal, metal oxide and polymer nanostructures on graphene surface. The surface modified dopants in graphene enhance the catalytic activity and facilitate the charge transfer mechanism.[15-18] However, during bioelectrode fabrication and drying process, graphene sheets agglomerates and restacks irreversibly to form graphite due to van der Walls interaction among individual graphene sheets.[19] This irreversible restacking of graphene layers significantly decreases the accessible surface area and hence lowers the enzyme immobilization site. So the analyte ions could access only the top and bottom of the stacked graphene layers. This blocks the diffusion of analyte to electrode interface leading to worse performance. In this regard, incorporation of conducting spacer plays a crucial role in separating graphene layers form restacking thereby preserving its accessible surface area which ultimately enhances its electrocatalytic activity and sensing properties.[20]It is demonstrated that inclusion of carbon nanotube between graphene layers improves both the effective surface area and the electrochemical properties of the graphene based composites. The large electrochemically active surface area allows effective enzymes immobilization, easy diffusion of analyte to electrode interface and promotes electron transfer mechanism.

Recently noble metal nanoparticles on graphene or MWCNTs surfaces have been reported as efficient sensing platform for their distinguished physical and chemical attributes like excellent biocompatibility, catalytic activity and chemical stability. The catalytic activity is highly size dependent and enhances with decreasing particle size.[21-24] Herein we report the fabrication of a H_2O_2 and enzymatic glucose biosensor platform combining synergetic assay of narrow sized Au nanoparticles (~3-4nm) decorated MWCNTs-sG hybrid nanocomposite. The large-scale synthesis of the material was done in a single step green technique using focused solar radiation. The synthesis procedure is facile, cost effective, environmental friendly and does not require any post synthesis treatments for purification. The synthesized material was characterized by different characterization techniques and employed as a robust transducer material for electrochemical detection of H_2O_2 and enzymatic glucose biosensing. The biosensor exhibits enhanced catalytic properties compared to only MWCNT-sG based matrix which is attributed to the interaction between Au nanoparticles with MWCNTs-sG support leading to better enzyme adhesion and hence better stability and fast response of the biosensor.

2. Experimental Methods

2.1 Materials

Flake graphite powder (99.99% SP-1, Bay carbon, average particle size 45 μm), chloroauric acid ($HAuCl_4.3H_2O$, 99.99%), glucose oxidase (GOD, type x-s from Aspergillusniger), D-(+)-glucose were purchased from Sigma Aldrich. Concentrated sulphuric acid (H_2SO_4, 99%), concentrated nitric acid (HNO3, 98%), potassium permanganate ($KMnO_4$) from Rankem Chemicals, India were used as received. Hydrogen peroxide (H_2O_2, 30% wt/V) was purchased from Fisher scientific. Sodium phosphate buffer solution (PBS, 0.1M, pH 7.4) was prepared using sodium

dihydrogen phosphate (NaH_2PO_4, 99.5%) and di-sodium hydrogen phosphate (Na_2HPO_4, 98%) using deionized water (DI water). The enzyme solution was prepared using PBS and kept at 4˚C for further use. All the chemicals used were of analytical reagent grade.All the electrochemical studied and synthesis has been done using ultrapure water (18.2 MΩ cm) from Millipore system.

2.2 Synthesis of materials

Graphite oxide was prepared by referring Hummers method using flake graphite as the precursor.[25] Briefly, about 46 ml of concentrated H_2SO_4 was cooled down to 0˚C in an ice bath. Flake graphite powder (2gm) was added in it slowly and allowed to stirrer for 15 minutes. Then $NaNO_3$ (1gm) were added to the suspension gradually and stirrer for 15 more minutes. About 6 gm of $KMnO_4$ was added to the above prepared mixture and allowed to cool down to room temperature by removing from ice bath followed by adding water to it. The suspension was again diluted by adding warm water. Then, 10 ml of H_2O_2 (30%) was added to it, which immediately turns the gray solution into bright yellow color. The suspension was filtered and washed thoroughly by copious amount of DI water and finally the residue was dried in vacuum oven at 60°C temperature. MWCNTs were prepared by catalytic chemical vapor deposition (CVD) technique using acetylene as a carbon precursor and rare earth based $MmNi_3$ (Mm = Misch metal) type alloy hydride catalyst.[26] The synthesized MWCNTs were air oxidized at 400°C followed by treatment with concentrated HNO_3 and H_2SO_4 (3:1) in order to remove amorphous carbon impurities and remaining metal catalyst particles.

Au-MWCNTs-sG was prepared in a simple green technique by simultaneous reduction and exfoliation of metal salt-GO mechanical mixture in presence of MWCNTs. In our earlier report, we discussed the synthesis of metal/metal oxide alloy nanostructures over MWCNTs using

focused sun light.[27] Briefly, as synthesized GO (100mg), MWCNTs (5mg) and $HAuCl_4$ (27 mg, calculated for 30wt% loading)was mixed using a mortar pastel for a homogeneous mixture. The mixture powder was spread on a glass petridis and focused sun light was allowed to fall on the mixture using a convex lens of 90 mm diameter. The intense focused solar radiation creates sudden rise in temperature (250-300˚C) in few seconds which helps in GO exfoliation and simultaneous reduction of metal salt to metal nanoparticles. An apparent volume expansion with release of gaseous by-products was observed which indicates in situ reduction of metal salt and GO to graphene. The presence of MWCNTs here acts like conducting spacer between graphene layers, which could enhance the effective accessible surface area of the hybrid composite and hence improves the electrochemical responses. For comparison purpose, we synthesized MWCNTs-sG composite by taking MWCNTs-GO mixture as starting material and following the above discussed procedure.

2.3 Materials characterization techniques

The crystallinity of the above-synthesized material was characterized by X-ray diffraction technique using PANalytica X'pert pro X-ray diffractometer with Cu-K_α as X-ray source. The morphology of the sample was studied by high-resolution transmission electron microscopy (HRTEM, Tecnai G^2 20 S-TWIN). The X-ray photoelectron spectra were recorded with SPECS X-ray Photoelectron Spectrometer using Mg K_α as X-ray source and PHOIBOS 100MCD energy analyser. All the XPS spectra were recorded at ultra high vacuum (10^{-10} mbar range) and data were analysed using CASA XPS software. The electrochemical studies were carried out by CH Instrument, electrochemical workstation with a three-electrode electrochemical cell comprising a glassy carbon electrode GCE (3 mm diameter) as working electrode, Pt wire counter electrode

andAg/AgCl (1M KCl solution) as reference electrode. PBS was used as supporting electrolyte for all electrochemical studies at ambient temperature.

2.4 Fabrication of the bioelectrodes

The bioelectrode was fabricated over glassy carbon electrode (GCE). Prior to each experimental study, GCE was polished mirror like using 1, 0.3 and 0.05 micron alumina slurry in sequence followed by rinsing thoroughly by DI water. The cleaned electrode was modified by simple drop casting method. Firstly, 5mg of Au-MWCNTs-sG hybrid composite was sonicated in 0.5ml nafion solution (0.5%). About 5µL aliquot was drop-casted on the shining surface of GCE and allowed to dry at room temperature. In the same way, MWCNTs-sG@ GCE was prepared for comparison studies taking same weight percentage as for Au-MWCNTs-sG@GCE. For enzyme electrode fabrication, 5µL of GOD enzyme solution (15mg/ml) was over coated on the modified electrode and allowed to dry and kept at 4˚C in order to preserve enzyme activity. Before each electrochemical study, the modified electrodes were thoroughly rinsed in DI water in order to remove loosely attached enzymes.

3. Results and Discussion

3.1 Material characterization

The electrochemical response is highly subjective to the surface morphology of sensing matrix. We studied the surface morphology of the hybrid composites by electron microscopy. Figure 1 shows the HRTEM images of Au-MWCNTs-sG (a, b & c) and MWCNTs-sG (d & e) composites at different resolutions. From the micrographs, it is clearly evident that the MWCNTs are well embedded with graphene sheets. The HRTEM images reveals that the narrow sized Au nanoparticles are homogeneously assembled over two-dimensional graphene and one-

dimensional MWCNTs without any particle aggregation. The particle size distribution of Au nanoparticles was calculated by taking different area in to count which is shown in figure 1(f). The average particle size appears to be ~3-4nm.The energy dispersive X-ray analysis (EDX) result demonstrates the presence of Au in the hybrid composite (shown in ESI, fig. S1).

The XRD pattern of the hybrid composite has been compared with the starting materials. Figure 2 depicts the XRD pattern of (a) MWCNTs, (b) GO, (c) MWCNTs-GO mixture, (d) MWCNTs-sG, (e) MWCNTs-GO-Au salt, and (f) Au-MWCNTs-sG. The diffraction peak appear around 26.56˚ in curve (a) can be indexed to C (002) peak of graphitic structures in MWCNTs. Being highly intercalated by oxygen containing functional groups in basal plane as well as edges, the C (002) peak in GO appears at 11˚ with an expanded *d* spacing of 0.84 nm. Again for MWCNTs-GO mixture, two C (002) diffraction peaks appear in the plot, which indicates the presence of both carbon nanostructures. After treating under solar radiation, a broad and sharp diffraction peak appears in a range from 17˚ to 30˚, which is the confirmation of complete conversion of GO to sG. The sharp peak at 26.53˚ corresponds to presence of MWCNTs in the hybrid composite however; the broadening depicts disorder in c-axis in sG. Again for a mixture of Au salt, MWCNTs and GO, many additional peaks appear along with C (002) diffraction peak indicating unreduced Au salt in the mixture. However, these peaks disappear completely after treating under solar radiation instead five crystalline peaks at 33.18, 44.38, 64.57, 77.56 and 81.72˚ (JCPDS No 65-2870) appear corresponding to cubic Au nanostructure along with C (002) peak. This indicates complete reduction of metal salt to crystalline metal nanoparticles and successful decoration over graphene and MWCNT.

The main advantage of the synthesis method is the complete reduction of gold salt to gold nanoparticles without producing any chemical residue, which is evident from the XPS survey

spectra of the samples discussed in figure 3 (A). For GO, O1s peak dominates over C1s indicating the presence of considerable amount of oxygen containing functional groups in GO. When reduced to graphene in solar reduction, most of the functional groups are removed due to high heating rate by intense solar radiation. This result a decrease in oxygen contain in MWCNT-sG hybrid. Similar trend was observed for O1s in Au-MWCMT-sG hybrid. Including this features, an additional doublet peak appears around 81-91eV, which corresponds to Au4f peak. Figure 3(B) shows the Au4f high-resolution spectrum of Au-MWCNTs-sG hybrid composite after back ground subtraction. The spectrum was deconvoluted into two sub picks at binding energy values 83.8eV and 87.5eVwhich arises due to spin orbit coupled level of $Au4f_{7/2}$ and $Au4f_{5/2}$respectively.In comparison to characteristics peak of metallic Au^0 with sub peaks at 84.0eV and 87.7eV, the peaks shift negatively towards lower BE values of ~0.2eV.[28] Being lower in work function, it is expected that the negative shift in binding energy can be due to electron transfer from graphene/MWCNT (W.F~4.7eV) to surface dispersed Au nanoparticles (W.F~5.31eV).[29] This depicts good stability of Au nanoparticles on sG/MWCNTs surface which intern restricts the particles from agglomeration. The absence of any other oxidation states of Au in the hybrid composite clearly depicts the complete reduction of gold salt over graphene and MWCNTs surface in solar reduction.

3.2 Electrochemical activity towards H_2O_2

H_2O_2 is an important analyte in many different fields such as food, clinical, pharmaceutical, environmental and industrial analysis.[30-31] Being a universal oxidant, it is often used in basic science research. Including this, being a measurable electroactive byproduct in enzymatic (GOD) glucose reaction, trace level detection of H_2O_2 is of great importance. Here we have systematically investigated the electrochemical response of the synthesized hybrid composite for

H_2O_2 sensing in N_2 saturated PBS. N_2 saturation is done in order to mimic the physiological levels of O_2 in PBS and avoid the reduction of superoxide species.[32-33] The electrochemical Figure 4 (A) shows the cyclic voltamogram for 5mM H_2O_2 in N_2 saturated PBS for Au-MWCNTs-sG@GCE(a) and MWCNTs-sG@GCE(b). For Au-MWCNT-sG@GCE, the reduction potential obtained at -0.2V is much less than that for MWCNTs-sG@GCE (-0.4V). This indicates Au-MWCNTs-sG has much electro catalytic activity towards H_2O_2 redox reaction which can be attributed to synergistic effect from well disperse narrow sized Au nanoparticles of on graphene and MWCNTs. Furthermore the effect of scan rates on the CV performance isstudied for both the electrodes (shown as insets). Figure 4(B and C) shows the variation of redox peak current (I_p) with scan ratefor Au-MWCNTs-sG@GCE and MWCNTs-sG@GCE. It is found that both the cathodic (I_{pc}) and anodic (I_{pa}) peak current increases linearly with scan rate. The linear regression coefficient (R^2) is calculated to be 0.999 from the linearly fitted plots for Au-MWCNTs-sG@GCE, whereas for MWCNTs-sG@GCE, the calculated R^2 value is 0.999 (for I_{pa}) and 0.998 (for I_{pc}).This suggests that the electrochemical reaction is a surface-controlled electrochemical process.[34-35]

The amperometric response of the electrode for successive addition of H_2O_2 is analyzed under optimal conditions. Figure5(D) shows the typical steady state current vs time (i-t)plot of Au-MWCNTs-sG@GCE carried out at in N_2 saturated PBS (pH 7) at a reduction potential of -0.2V.When an aliquot of H_2O_2 was added to the buffer solution under constant stirring conditions, the reduction current increased quickly to achieve stable value before further addition. The response time (time required to achieve ~99% of steady state current) is calculated from i-t plot, which is less than 1s (fig. S3, ESI). It depicts a fast amperometric response behavior, which can be due to easy diffusion of H_2O_2 through modified electrode assembly and

fast electron transfer at Au-MWCNTs-sG@GCE interface. This result is better than recent reports for graphene based composite (response time < 3s), gold nanoparticles-CNT electrode (response time <5s), graphene wrapped Cu_2O nanocubes (response time < 9s).[36-38] Inset of figure 3(D) shows the calibration curve for the biosensor which gives a linear regression range from 1mM to 62 mM with linear regression coefficient R^2=0.996 . The limit of detection (LOD) is calculated to be 13μM at signal-to-noise ratio(S/N) of 3.

3.3 Electrochemical activity towards Glucose

Based on the enhanced electrochemical performance of Au-MWCNTs-sG@GCE for H_2O_2 detection, we further employed the modified electrode for enzymatic glucose sensing. The enzyme electrode was prepared as discussed before by immobilizing GOD enzyme on Au-MWCNTs-sG@GCE. The glucose sensing mechanism is based on GOD catalyzed selective oxidation of glucose in presence of O_2 to form H_2O_2. Further the probe can be electrochemical oxidation/reduction current to measure the concentration of glucose. Figure S4 (ESI) shows the CVs for GOD-Au-MWCNTs-sG@GCE taking 5mM glucose solution in O_2 saturated PBS and varying scan rate (insets). It is observed that both the I_{pc} and I_{pa} increases linearly with scan rate and the linear regression coefficient (R^2) is calculated to be 0.999 for both the linearly fitted plots. The response of GOD-Au-MWCNTs-sG@GCE was recorded for repeated addition different glucose concentration in 20s interval of time. Figure 5(A) shows the i-t plot on successive addition of 0.3, 0.5 and 1mM glucose. When an aliquot of glucose (1mM) was added to homogeneously stirred PBS, a current increase of ~5μA was observed and it reaches a stable value. After reaching up to 20mM glucose a plateau current is observed deviating from linear stepwise increase. Figure 5(B) depicts the calibration plot obtained from i-t response. It shows wide range linearity from 50μM to 20mM glucose concentration with linear regression

coefficient (R^2) of 0.996. The detection limit is calculated from the linearly fitted calibration plot which is 2.48μM. Further the enzyme substrate affinity is investigated from Michelis-Menton enzyme kinetics.[39] The apparent Michelis-Menton constant (K_m^{app}), which gives an apparent affinity of the substrate towards the enzyme, is calculated using the following Line weaver-Burk equation.

$$1/I_{ss} = K_m^{app}/I_{max}C + 1/I_{max}$$

where I_{ss} is the steady state current after addition of glucose, I_{max} is the saturation current and C is glucose concentration. The value of K_m^{app} for GOD-Au-MWCNTs-sG@GCE estimated from Figure 4(B) to be 1.07mM. The smaller value reflects GOD adsorbed on Au-MWCNTs-sG hybrid matrix has stronger affinity of towards glucose. Again the amperometric response was recorded at each addition of 0.3mM and50μM aliquot of glucose, which is shown in figure 5(C and D). The plots of I_p vs. concentration fit linearly with R^2 value 0.997and 0.995respectively.

The stability of the GOD-Au-MWCNTs-sG@GCE sensor was investigated by measuring the signal durability for 2mM glucose over a long period of 3400 s. As shown in figure 6(A), a very less (<5%) current lose was observed which depicts very good stability of the biosensor. The insets show the plot representing the response time (time required to achieve ~99% of steady state current) of the sensor which is derived from i-t plot. It shows that the current stabilizes in no more than 0.1s indicating excellent and rapid amperometric response behavior. The stability, response time and linearity of our sensor are greatly superior than similar graphene/MWCNT based glucose sensors. This could be due to the presence of MWCNTs in the sensing matrix which can act as conducting spacer in between graphene layers and takes a major role in facilitating fast electron transfer between electrode and adsorbed enzyme. The performance of

our biosensor is compared with similar existing glucose biosensors based on metal NP graphene/MWCNT based sensing matrix, which is shown in Table 1.

The interference from coexisting bimolecular species like uric acid, ascorbic acid, dopamine, greatly influences the performance. In order to test the selectivity of the fabricated biosensor, we measured the current response by repeatedly adding 1mM glucose in the presence of UA, AA and DA, which is shown in figure6(B). For successive addition of 1mM glucose, the sensor gave remarkable and repeatable current response. After adding 0.1mM UA, AA and 0.5mM DA, the current response was trivial. Again adding glucose the current response was repeatable. However, a very small current (<5% of current due to glucose oxidation) is observed for AA, which can be due to its low oxidation potential. No significant enhancement in interference current is observed instead it gave good response for each addition of 1M aliquot of glucose. This reveals excellent selectivity of the present biosensor.

For practical application and commercialization, a reproducible and long-term stable glucose sensor is highly desirable. The reproducibility and stability of the biosensor was studied by measuring the amperometric response periodically for 1mM glucose concentration. In order to preserve enzyme activity the sensor was stored at 4˚C when not in use. After one week, the sensor could recover 99% of current in amperometry study. This signifies good reproducibility of our biosensor.

4. Conclusion

In summary, well-dispersed Au nanoparticles on graphene-carbon nanotube hybrid composite was synthesized by a green solar energy-reduction technique. The fabricated Au-MWCNTs-sG biosensor exhibits high electro catalytic activity for H_2O_2 over a wide linear range from 1mM to

62mM, a low detection limit of 13μM with a response time less than 1s. When employed for enzymatic glucose detection, it shows a better enzyme affinity, with a linearity of 50μM – 20mM and with a detection limit of 2.48μM. For glucose, the sensor exhibits a very fast response with response time ~0.1s. Compared to similar graphene and MWCNT based biosensors already developed the present one depicts enhanced performance in the point of rapid response, wide range linearity, better selectivity, stability and low detection limit. The combination of these unique characteristic properties of the present sensor finds it as a potential competitor in electrochemical biosensing.

Table 1 Comparison of performance of glucose biosensors based on graphene/MWCNT as sensing matrix.

Glucose biosensor	Linear range (mM)	Detection limit (μM)	Response time (sec)	Reference
Au-MWCNT-sG	0.05-20	2.48	< 1	present work
GOD-GR-CS	0.08 - 12	20	-	15
Pd-ERGO	0.025- 4.9	0.56	5	18
AuNP-GR-CS	2- 14	180	-	21
GQD	0.005- 1.27	1.73	3	40
ERGO-MWNT	0.01- 6.5	4.7	-	41
AuNP-MWCNT	0.1-10	6.7	7	42
Pt-CNT	0.16-11.5	55	5	43

Acknowledgement: We thank Indian Institute of Technology Madras, Chennai, for financial support.

Figure captions:

Figure 1 High resolution transmission electron microscope (HRTEM) images of Au-MWCNTs-sG (a, b and c) and MWCNTs-sG (d and e) at different resolutions. (f) Histogram representing the size distribution of Au nanoparticles.

Figure 2 X-ray diffraction pattern of (a) pure MWCNTs, (b) GO, (c) mechanically mixed GO and MWCNTs, (d) MWCNTs-sG, (e) mechanically mixed MWCNTs, GO, and Au salt and (f) Au-MWCNTs-sG.

Figure 3 (A) XPS survey spectrum of (a) GO, (b) MWCNTs-sG and (c) Au-MWCNTs-sG. (B) Deconvoluted high-resolution X-ray photoelectron (XPS) spectra of Au4f in Au-MWCNTs-sG hybrid composite.

Figure 4(A) Cyclic voltametry response of (a) Au-MWCNTs-sG@GCE and (b) MWCNTs-sG@GCE for 5mM H_2O_2 inN_2 saturated PBS at 50mV/s scan rate. (B and C) Plot of peak current vs scan rate for MWCNTs-sG@ GCE and Au-MWCNTs-sG@GCE. Insets: (in both B and C) show the CVs at different scan rates. (D) Amperometric (i-t) response to successive addition of H_2O_2 for Au-MWCNTs-sG@GCE at -0.2V in N_2 saturated PBS (0.1M) Inset: (in D) linearly fitted calibration curve (steady state current vs H_2O_2 concentration) obtained from the amperometric i-t analysis.

Figure 5(A) Amperometric (i-t) responses to successive addition of glucose for GOD-Au-MWCNTs-sG@GCE at 0.2V in O_2saturated PBS. (B) The calibration curve (steady state current versus glucose concentration) and the Lineweaver-Burk plot (current^{-1} versus glucose concentration^{-1}) obtained from the amperometric response (in A). (C and D) Amperometric response for successive addition of 0.3mM glucose and 50μM glucose in O_2 saturated PBS. Insets: (in C and D) corresponding linearly fitted calibration plots.

Figure 6(A) Amperometric response of the GOD-Au-MWCNTs-sG@GCE to 2 mM glucose in 0.1 M PBS over a long period of running time of 3400 s. (B) Amperometry i-t plot for GOD-Au-MWCNT-sG@GCE on successive addition of 1mM glucose followed by addition of 0.1mM AA, 0.1 mM UA and 0.5 mM DA at 0.2V in O_2 saturated PBS.

References:

1. Clark, L. Jr.; Lyons, C. *Ann. NY Acad. Sci.***1962***, 102,* 29-45.
2. Turner, A. P. F. *Chem. Soc. Rev.* **2013***, 42,* 3184-3196.
3. Liu, Y.; Wang, M.; Zhao, F.; Xu, Z.; Dong, S.*Biosens. Bioelectron.***2005***,21,* 984-988.
4. Jia, X.; Hu, G.; Nitze, F.; Barzegar, H. R.; Sharifi, Tiva; Tai, C. W.; Wagberg, T.*ACS Appl. Mater. Interfaces***2013***, 5,* 12017-12022.
5. Cui, H-F.; Ye, J. S.; Liu, X.; Zhang,W.D.; Sheu, F. S.*Nanotechnology***2006***, 17,*2334-2339.
6. Yang, W.; Ratinac, K. R.; Ringer, S. P.; Thordarson, P.; Gooding, J. J.; Braet, F.*Angew. Chem. Int. Ed.***2010***, 49,* 2114-2138.
7. Cai, C.; Chen, J.*Anal. Biochem.* **2004***, 332,* 75-83.
8. Agu, L.; Yanez-Sedeno, Paloma; Pingarron, Jose M.*Anal. Chim. acta***2008***,622,* 11-47.
9. Zhu, Z.; Garcia, G. L.; F., A. J.; Xie, H.; Moussy, F.; Milne, W. I. *Sensors* **2012***, 12,* 5996-6022.
10. Rivas, G. A.; Rubianes, M. D.; Rodr´ıguez, M. C.; Ferreyra, N. F.; Luque, G. L.; Pedano, M. L.; Miscoria, S. A.; Parrado, C. *Talanta***2007***, 74,* 291-307.
11. Balandin, A. A.; Ghosh, S.; Bao, W.; Calizo, I.; Teweldebrhan, D.; Miao, F.; Lau, C. N. *Nano Lett.***2008***,8,* 902-907.
12. Castro Neto, A. H.; Guinea, F.; Peres, N. M. R.; Novoselov, K. S.; Geim, A. K. *Rev. Mod. Phys.* **2009***, 81,* 109-162.
13. Kamat, P. V. Graphene-Based Nano assemblies for Energy Conversion. *J. Phys. Chem. Lett.* **2011***, 2,* 242-251.
14. Pumera, M. *Chem. Soc. Rev.***2010***, 39,* 4146-4157.

15. Kang, X.; Wang, J.; Wu, H.; Aksay, I. A.; Liu, Jun.; Lin, Y. *Biosens. Bioelectron.***2009**, *25,* 901-905.

16. Luo, Z.; Yuwen L.; Han, Y.; Tian, J.; Zhu, X.; Weng, L.; Wang, L. *Biosens. Bioelectron.***2012**, *36,* 179-185.

17. Jiang, F.; Yue, R.; Du, Y.; Xu, J.; Yang, P. *Biosens. Bioelectron.***2013**,*44,*127-131.

18. Qin, Y.; Kong, Y.; Xu, Y.; Chu, F.; Tao, Y.; Li, S.*J. Mater. Chem.***2012**, *22,* 24821-24826.

19. Yang, S. Y.; Chang, K. H.; Tien, H. W.; Lee, Y. F.; Li, S. M.; Wang, Y. S.; Wang, J. Y.; Ma, C. C. M.; Hu, C. C. *J. Mater. Chem.* **2011**, *21,* 2374-2380.

20. Wang, Y.; Wu, Y.; Huang, Y.; Zhang, F.; Yang, X.; Ma, Y.; Chen, Y. *J. Phys. Chem. C***2011**, *115,* 23192-23197.

21. Shan, C.; Yang, H.; Han, D.; Zhang, Q.; Ivaska, A.; Niu, L. Biosens. Bioelectron.**2009**, *25,* 1070-1074.

22. Jans, H.; Huo, Q. *Chem. Soc. Rev.* **2012**,*41,* 2849-2866.

23. Sharma, S.; Gupta, N.; Srivastava, S.Biosens. Bioelectron.**2012**, *37,* 30-37.

24. Zhou, X.; Xu, W.; Liu, G.; Panda, D.; Chen, P. *J. Am. Chem. Soc.***2010**,*132,* 138-146.

25. Hummers, W. S.; Offeman, R. E. *J. Am. Chem. Soc.***1958**, *80,* 1339-1339.

26. Reddy, A. L. M.; Shaijumon, M. M.; Ramaprabhu, S. *Nanotechnology* **2006**, *17,* 5299-5305.

27. Baro, M.; Nayak, P.; Baby, T. T.; Ramaprabhu, S. *J. Mater. Chem. A***2013**,*1,* 482-486.

28. Velamakanni, A.; Magnuson, C. W.; Ganesh, K. J.; Zhu, Y.; An, J.; Ferreira, P. J.; Ruoff, R. S. *ACS Nano* **2010**, *4,* 540-546.

29. Benayad, A.; Shin, H. J.; Park, H. K.; Yoon, S. M.; Kim, K. K.; Jin, M. H.; Jeong, H. K.; Lee, J. C.; Choi, J. Y.; Lee, Y. H. *Chem. Phys. Lett.***2009**,*475,* 91-95.

30. Barrington, D. J.; Ghadouani, A. *Environ. Sci. Technol.***2008***, 42,* 8916-8921.

31. Prodromidis, M. I.; Karayannis, M. I. *Electroanalysis* **2002***, 14,* 241-261.

32. Shao, M.; Liu, P.; Adzicgvjuj, R. R. *J. Am. Chem. Soc.* **2006**, *128*, 7408-7409.

33. Sardesai, N. P.; Andreescu, D.; Andreescu, S. *J. Am. Chem. Soc.* **2013**, *135*, 16770-16773.

34. Bird, A. J.; Faulkner, L. R. 20102nd ed. John Wiley & Sons, Inc.: New York.

35. Song, J.; Xu, L.; Zhou, C.; Xing, R.; Dai, Q.; Liu, D.; Song, H. *ACS Appl. Mater. Interfaces* **2013***, 5,* 12928-12934.

36. Zhang, Y.; Liu, Y.; He, J.; Pang, P.; Gao, Y.; Hu, Q. *ElectrochimicaActa***2013***, 90,* 550-555.

37. Chen, K. J.; Lee, C. F.; Rick, J.; Wang, S. H.; Liu, C. C.; Hwang, B. J. *Biosens. Bioelectron.* **2011***, 33,* 75-81.

38. Liu, M.; Liu, R.; Chen, W. *Biosens. Bioelectron.***2013***, 45,* 206-212.

39. Pradhan, D.; Niroui, F.; Leung, K. T *ACSAppl. Mater. Interfaces***2010***, 2,* 2409-2412.

40. Razmi, H.; Rezaei, R. M.;*Biosens. Bioelectron.***2013**, *41*, 498-504.

41. Mani, V.; Devadas, B.; Chen, S. M. *Biosens. Bioelectron.***2013***, 41,* 309-315.

42. Wu, B. Y.; Hou, S. H.; Yin, F.; Zhao, Z. X.; Wang, Y. Y.; Wang, X. S.; Chen, Q..*Biosens. Bioelectron.* **2007**, *22*, 2854-2860.

43. Wen, Z.; Ci, S.; Li, J. *J. Phys. Chem. C* **2009**, *113*, 13482-13487.

Figure 1.

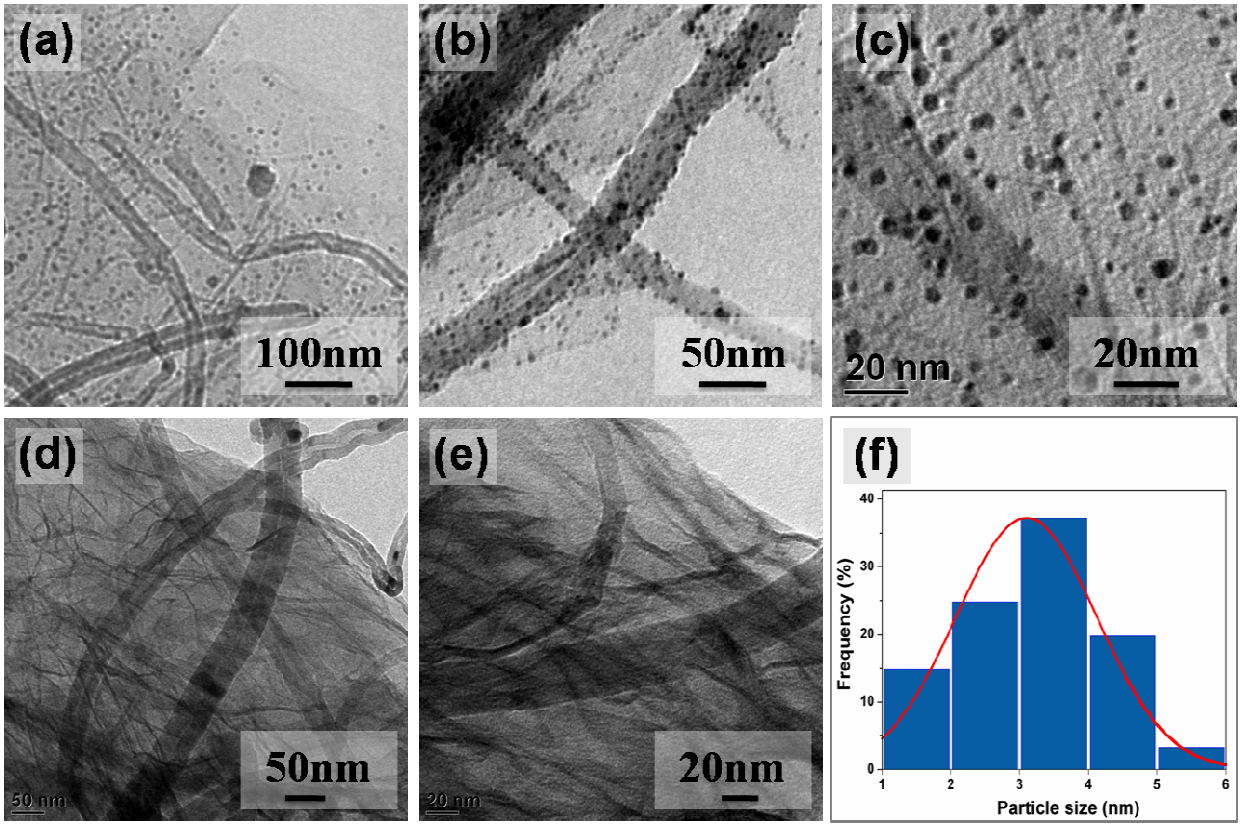

Figure 2.

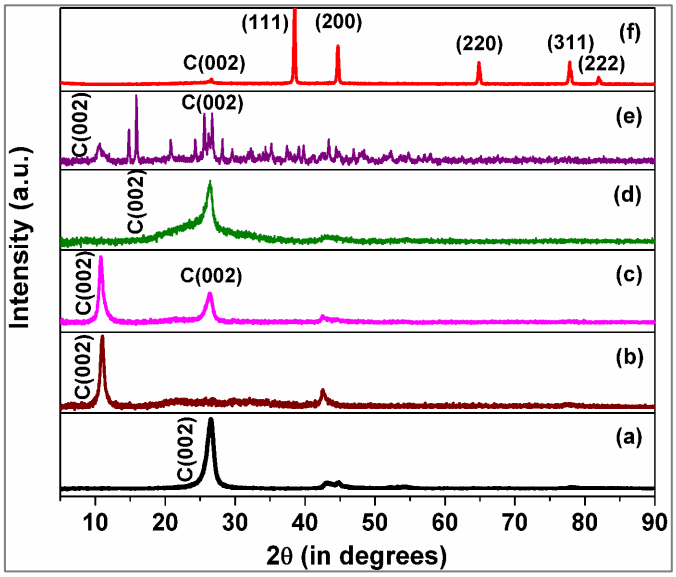

Figure 3.

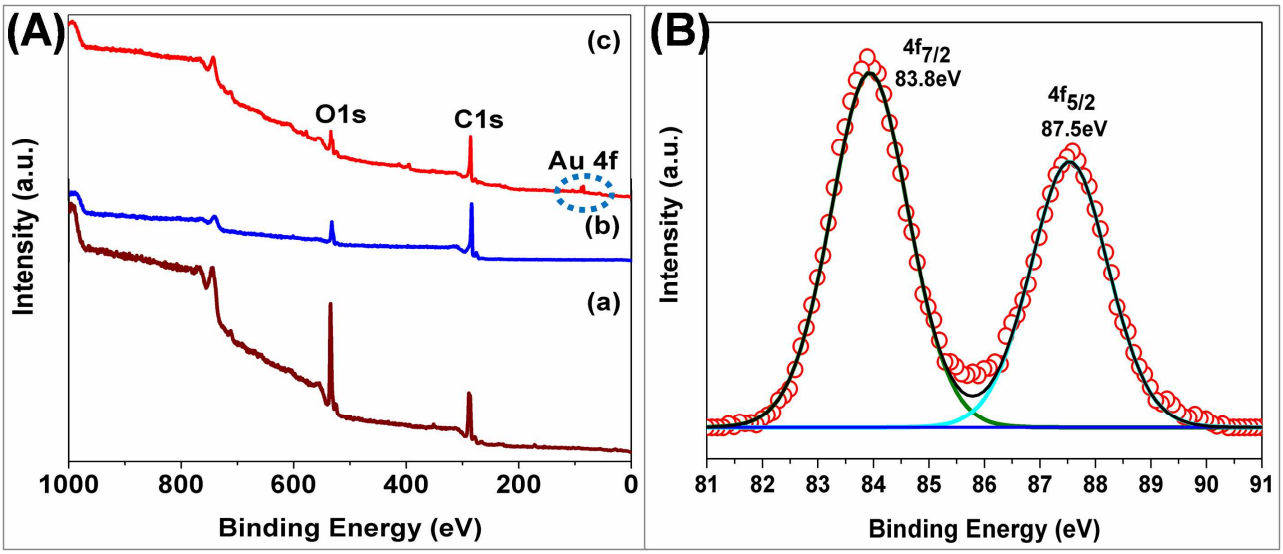

Figure 4.

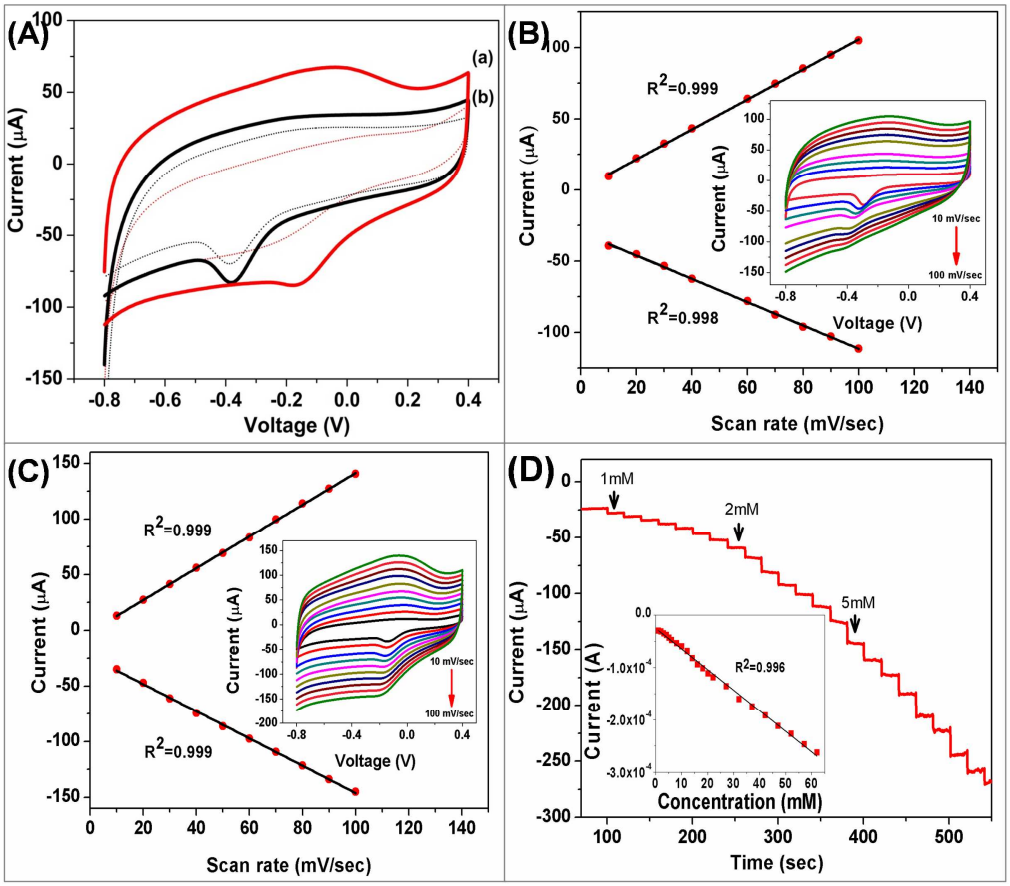

Figure 5.

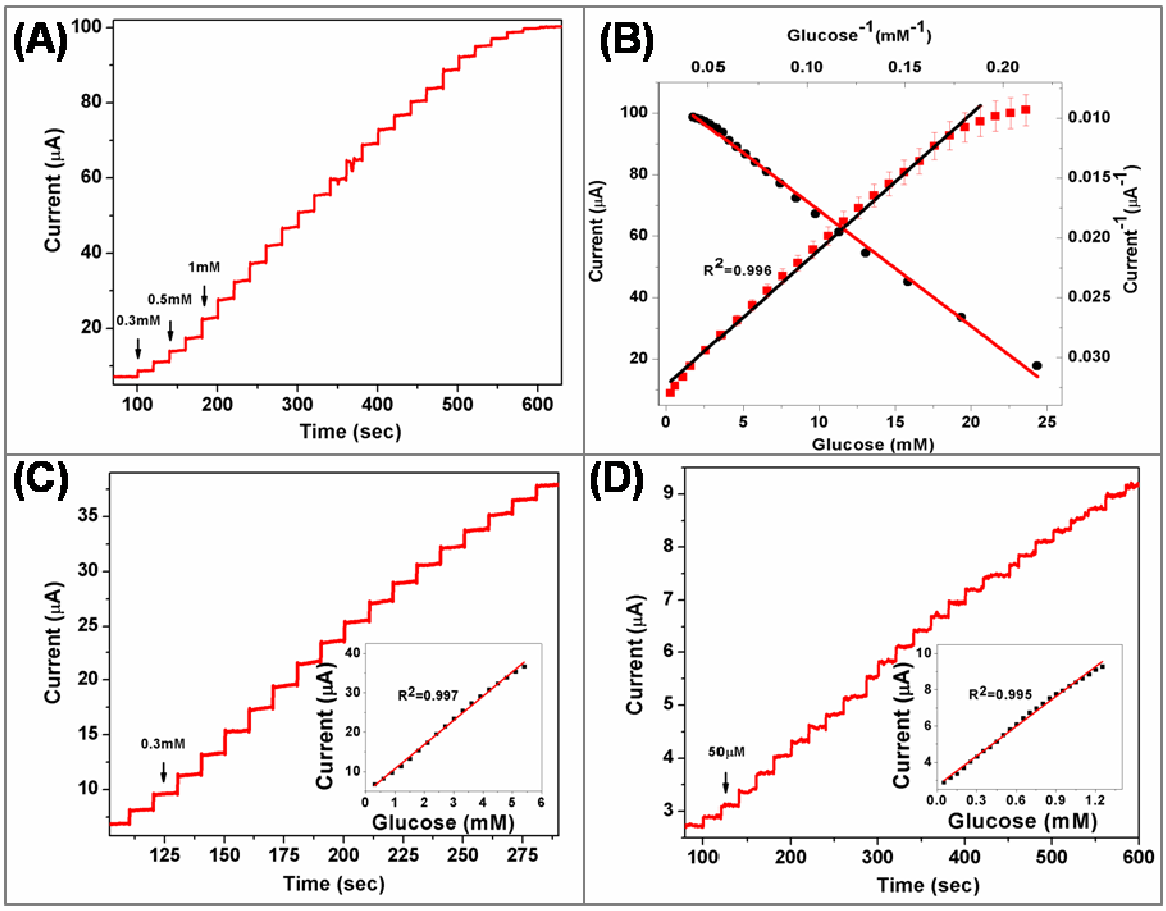

Figure 6.

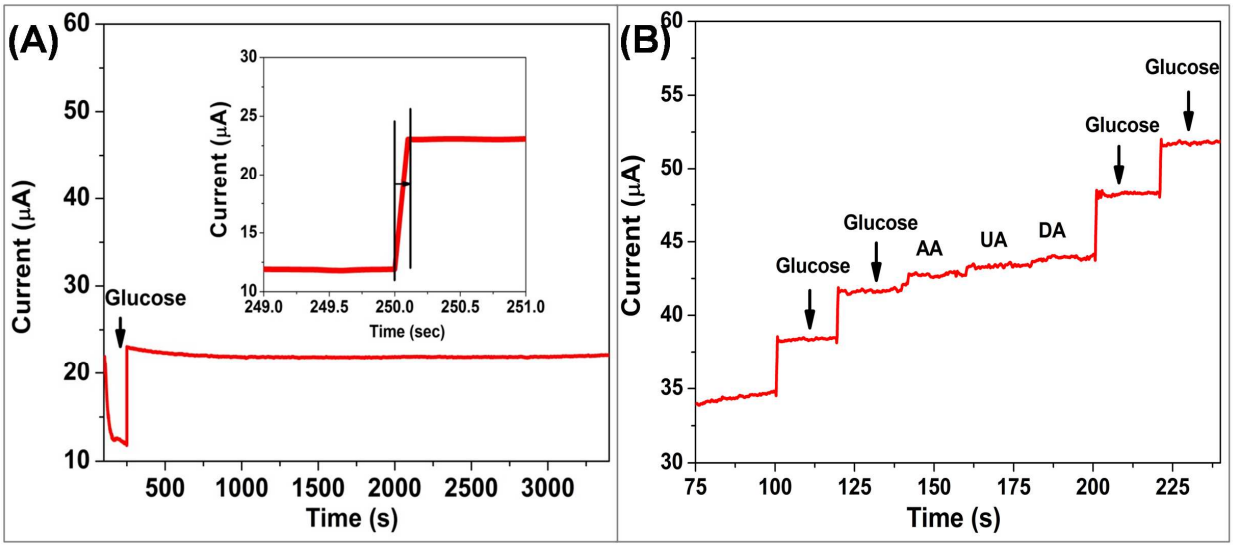

TOC